Published in final edited form as:
Mol Cancer Ther. 2013 October ; 12(10): 2176–2186. doi:10.1158/1535-7163.MCT-12-1210.

EGFR Inhibition Promotes an Aggressive Invasion Pattern Mediated by Mesenchymal-like Tumor Cells within Squamous Cell Carcinomas

Devraj Basu[1,6,7], **Arnaud F. Bewley**[1], **Steven M. Sperry**[1], **Kathleen T. Montone**[2], **Phyllis A. Gimotty**[3], **Kati Rasanen**[6], **Nicole D. Facompre**[1,6], **Gregory S. Weinstein**[1], **Hiroshi Nakagawa**[4], **J. Alan Diehl**[5], **Anil K. Rustgi**[4], and **Meenhard Herlyn**[6]

[1]Department of Otorhinolaryngology-Head and Neck Surgery, University of Pennsylvania, Philadelphia, PA

[2]Department of Pathology and Laboratory Medicine, University of Pennsylvania, Philadelphia, PA

[3]Department of Epidemiology and Biostatistics, Center for Clinical Epidemiology and Biostatistics, Abramson Cancer Center, University of Pennsylvania, Philadelphia, PA

[4]Department of Medicine and Genetics, Division of Gastroenterology, Abramson Cancer Center, University of Pennsylvania, Philadelphia, PA

[5]Department of Cancer Biology, Abramson Cancer Center, University of Pennsylvania, Philadelphia, PA

[6]The Wistar Institute, Philadelphia, PA

[7]VA Medical Center, Philadelphia, PA

Abstract

Squamous cell carcinomas (SCCs) with an infiltrative invasion pattern carry a higher risk of treatment failure. Such infiltrative invasion may be mediated by a mesenchymal-like subpopulation of malignant cells that we have previously shown to arise from epithelial to mesenchymal transition (EMT) and resist epidermal growth factor receptor (EGFR) targeting. Here we demonstrate that SCCs with infiltrative, high risk invasion patterns contain abundant mesenchymal-like cells, which are rare in tumors with low risk patterns. This cellular heterogeneity was modeled accurately in three dimensional culture using collagen-embedded SCC spheroids, which revealed distinct invasive fronts created by collective migration of E-cadherin-positive cells versus infiltrative migration of individual mesenchymal-like cells. Because EGFR expression by mesenchymal-like cells was diminished in the spheroid model and in human SCCs, we hypothesized that SCCs shift toward infiltrative invasion mediated by this subpopulation during anti-EGFR therapy. Anti-EGFR treatment of spheroids using erlotinib or cetuximab enhanced infiltrative invasion by targeting collective migration by E-cadherin-positive cells while sparing mesenchymal-like cells; by contrast, spheroid invasion in absence of mesenchymal-like cells was abrogated by erlotinib. Similarly, cetuximab treatment of xenografts containing mesenchymal-like cells created an infiltrative invasive front comprised of this subpopulation, whereas no such shift was observed upon treating xenografts lacking these cells. These results implicate mesenchymal-like SCC cells as key mediators of the infiltrative invasion seen in tumors with locally aggressive behavior. They further demonstrate that EGFR inhibition can promote an

Co-corresponding Authors: Meenhard Herlyn and Devraj Basu The Wistar Institute 3601 Spruce Street Philadelphia, PA, 19104 Phone: 215 898-3950; Fax: 215 898-0980; herlynm@wistar.org; devraj.basu@uphs.upenn.edu..

Conflicts of Interest: All authors declare no conflict of interest related to this work.

infiltrative invasion front comprised of mesenchymal-like cells preferentially in tumors where they are abundant prior to therapy.

Keywords

pattern of invasion; EGFR inhibition; squamous cell carcinoma; EMT; tumor heterogeneity

Introduction

Squamous cell carcinomas (SCCs) of the head and neck (1-4), esophagus (5, 6), and other sites (7, 8) exhibit variable histologic patterns of invasion that are associated with distinct clinical behaviors. These patterns comprise a spectrum ranging from well-demarcated invasive fronts amenable to close margin excision to stromal interfaces deeply infiltrated by individual malignant cells and thus requiring wide surgical margins for clearance. While conventional histologic grading of SCCs offers limited prognostic information (9, 10), an infiltrative pattern of invasion independently predicts a higher risk of local recurrence after surgical excision (1, 4, 7) and diminished overall survival (2, 4-6). A scoring system stratifying local recurrence risk for head and neck SCCs has been validated by Brandwein-Gensler et al. and is based on two infiltrative, high risk invasive patterns and three non-infiltrative, low risk patterns (1). However, the cellular differentiation events that underlie formation of high versus low risk invasion patterns are poorly defined. Molecular understanding of the differentiation states that determine invasion pattern may guide both surgical margin management and selection of targeted therapies against SCCs of distinct invasive subtypes.

The variable degrees of squamous differentiation observed among SCCs are also often evident within individual tumors. Such heterogeneity within a tumor predicts that the relative representation of tumor cell subpopulations with differing migratory behaviors will impact upon the structure of the invasive front. To dissect a key component of this heterogeneity, our prior studies focused on a subpopulation of cells within SCCs arising from partial epithelial to mesenchymal transition (EMT) (11, 12). These studies have shown that EMT creates cellular heterogeneity within SCCs by producing a subset of carcinoma cells with a broadly mesenchymal-like gene expression profile. These mesenchymal-like cells are represented within certain SCC cell lines, where they arise from E-cadherin-positive tumor cells undergoing EMT, acquire multiple mesenchymal markers including vimentin, down-regulate EGFR, and show resistance to cytotoxic and EGFR-targeted drugs (11, 12). A central role for these cells in SCC progression is supported by association of EMT with multiple aggressive carcinoma traits, including infiltrative invasion (13, 14), a reactive stroma (15), metastasis (16), and a stem cell-like phenotype (17). However our inability to detect mesenchymal-like cells in some SCC cell lines and human tumors supports that carcinoma invasion can be driven by other cell phenotypes and does not strictly require their presence.

The mechanisms that regulate formation of high versus low risk invasion patterns likely are closely linked to the diverse migratory behaviors exhibited by SCC cells. Specifically, carcinoma cells can invade in an EMT-independent mode by collective migration, which maintains cell surface E-cadherin expression within adherens junction-mediated contacts to create large clusters of cells invading as a pushing front (18). Alternately, cell surface E-cadherin loss, a pivotal event in the EMT program, permits isolated cells lacking adherens junctions to invade using either amoeboid or mesenchymal migratory modes (19). In head and neck SCCs, EMT predominantly facilitates the mesenchymal mode (20), a Rac GTPase dependent process distinguished from amoeboid movement by elongated fusiform cell

morphology, lack of actomyosin contractility, and remodeling of the extracellular matrix (19-21).

Targeting growth factor signaling has the potential to limit tumor growth while simultaneously promoting invasion and metastasis, with a notable example being anti-VEGF therapy, which increases invasion of multiple cancer types in preclinical models (22). For SCCs, a molecular understanding of epidermal growth factor receptor (EGFR) dependence has led to application of targeted anti-EGFR therapeutics, which show clinical efficacy that is significant albeit generally modest (23). Among the diverse mechanisms of resistance to EGFR inhibitors, EMT has been commonly implicated in non-small cell lung cancer and head and neck SCCs (24-29), and we have accordingly demonstrated an intrinsic resistance of a mesenchymal-like subpopulation to EGFR targeting (11). We therefore hypothesized that a shift toward an infiltrative invasion pattern would be mediated by differential effects of EGFR targeting upon E-cadherin-positive cells versus mesenchymal-like cells, based upon the distinct migratory mechanisms available to these two subpopulations.

Here we provide evidence of widely disparate content of mesenchymal-like tumor cells in human SCCs with high versus low risk invasion patterns. Using collagen-embedded tumor spheroids to model the distinct invasive fronts produced by E-cadherin-positive versus mesenchymal-like cells, we demonstrate how anti-EGFR therapy alters invasion pattern by selecting for cells with a distinct migratory behavior.

Materials and Methods

Cell lines and Clinical Specimens

Cell lines were maintained in 1:1 Dulbecco's modified Eagle and Ham's F12 media, with 400 ng/ml hydrocortisone, 10% fetal calf serum, and 50μg/ml gentamycin. OCTT2 and LNT14 cell lines were generated from patient-derived xenografts (PDXs), as described previously (11). SCC13 cells were obtained from the ATCC. Cell lines were authenticated with an Identify Mapping Kit (Coriell Institute, Camden, NJ, USA). Clinical specimens and data were obtained with informed consent, in compliance with University of Pennsylvania IRB protocol #417200 or Philadelphia VA Medical Center IRB protocol #010190.

Proliferation assay

MTS assays were performed using an aqueous cell proliferation assay kit per manufacturer instructions (Promega, Madison, WI). 2,500 cells per well (OCTT2, LNT14) or 5,000 cells per well (SCC13) were seeded in 96 well plates 24 hours prior to addition of drug, and growth was quantified after 72 hours of erlotinib exposure. Optical density was measured at 590nm (OD-590 nm) and normalized relative to OD-590 nm for DMSO controls.

Spheroid assays

Collagen-embedded spheroids were formed and treated by the liquid overlay method, as described previously (30). Briefly, 2500 cells/well were seeded in 1.5% agar-coated U-bottom 96 well plates and incubated for 72 hours to allow aggregation into individual spheroids. Spheroids were then harvested, seeded to 24 well plates as a suspension of 16 spheroids/well in bovine collagen I matrix, and overlaid with medium containing drug for 72 hours. For live-dead assays, treated spheroid cultures were incubated with calcein-AM and ethidium homodimer-1 for 1 hour at 37^{o}C, using a LIVE/DEAD Viability/Cytotoxicity Kit (Invitrogen, Carlsbad, CA). Collagen matrixes were inverted onto glass slides for confocal imaging.

Immunohistochemistry

Immunohistochemistry (IHC) was performed on 5μm paraffin sections by described methods (31). Antigens were retrieved by microwaving at pH 6.0 in 10mM citric acid. Mouse anti-human vimentin (1:500, Dako, Carpinteria, CA) and rat anti-E-cadherin (1:250, Invitrogen) primary antibodies were applied simultaneously. E-cadherin staining was detected using biotinylated anti-mouse IgG (1:250), Vectastain Elite ABC Reagent, and DAB Substrate kit. Subsequently, vimentin staining was detected using biotinylated anti-rat IgG (1:500), Vectastain ABC-AP Reagent, and Vector Red Substrate kit (Vector, Burlingame, CA). Slides were counterstained with hematoxylin.

Immunofluorescence and flow cytometry

Antigen retrieval and primary antibody application for immunofluorescence (IF) staining of PDX sections was performed as for IHC, using mouse anti-human vimentin (1:500, Dako), rabbit anti-Zeb1 rabbit antiserum (1:1000)(32), and/or rabbit anti-EGFR (1:100, Santa Cruz Biotech, Santa Cruz, CA). Primary antibodies were detected using Cy5 donkey anti-mouse IgG and Cy2 donkey anti-rabbit IgG (1:600, Jackson, West Grove, PA). Conventional and spheroid cultures were stained as described previously (11) using rabbit anti-vimentin (1:100, Anaspec, Fremont, CA) as well as directly conjugated Alexafluor 488 mouse anti-E-cadherin or mouse anti-EGFR (1:100, BD, San Jose, CA). Vimentin staining was detected with secondary alexafluor 568 anti-rabbit IgG (1:500, Invitrogen). Nuclei were stained with 4',6-diamidino-2-phenylindole (DAPI) throughout. Fluorescence activated cell sorting (FACS) for detection or purification of E-cadherin-positive cells was performed as described previously (11).

In vivo experiments

Non-obese diabetic/severe combined immunodeficient/interleukin-2 receptor γ-chain-deficient (NSG) mice were bred and used at the Wistar Institute animal facility under protocols approved by the Institutional Animal Care and Use Committee. PDXs were generated from human SCC specimens as described previously (11) and analyzed histologically after 2-4 passages. Xenografts of OCTT2 and SCC13 cell lines were generated by subcutaneous injection of 1×10^6 cells in 100 μl Matrigel (BD, Franklin Lakes, NJ). Tumor volumes were measured as [length × width^2]. For drug treatment, 1mg cetuximab (Imclone, New York, NY) or equivalent volume saline control was injected intraperitoneally every 3 days.

Microscopy and image analysis

Fluorescent imaging of spheroids was performed using either a spinning disk confocal Nikon Eclipse Ti-U microscope and iVision software or a Leica TCS SP5 II laser scanning confocal microscope and Leica LAS software. Other light and IF images were obtained using Nikon TE2000 inverted or E600 upright microscopes and processed with ImagePro-Plusv6.2 or ACT-1 software. Pseudocoloring of IHC and IF micrographs and subsequent image-based quantitative analysis of E-cadherin versus vimentin staining areas in these images was performed using ImagePro-Plus as detailed previously (11). The percentage of Zeb-1 positive nuclei with vimentin positive cytoplasm was defined in three 40x fields containing vimentin-positive areas and expressed as means with standard deviation. Within each experiment, uniform image acquisition settings were used, and images were batch processed to ensure unbiased comparison among samples. Pattern of invasion assessment using the Brandwein-Gensler system (1) was reviewed by a head and neck pathologist (KT Montone).

Statistical analysis

Groups were compared in fig. 1B and 4C using a one-way ANOVA. In 1B, the natural logarithm of area was used to make variances between groups more similar. In fig. 5A, tumor volumes over time were compared using a two-way mixed ANOVA. In these analyses involving multiple comparisons, adjusted p-values were computed using Tukey's procedure. In fig. 5C, differences in % staining area between groups were evaluated with a t-test using Satterthwaite's method to adjust for unequal variances. Data with error bars represent mean ± standard error of mean.

Results

PDXs of human SCCs with infiltrative invasion contain abundant mesenchymal-like cells

Using the Brandwein-Gensler risk stratification system for SCC pattern of invasion (1, 3, 4), four infiltrative, high risk tumors and six low risk tumors were identified in a panel of ten resected, advanced stage head and neck SCCs with diverse clinical and pathologic traits (supplementary table S1). To facilitate detection of mesenchymal-like tumor cells and comparison of their frequency between high and low risk groups, primary human tumors were directly passaged as PDXs in NSG mice. By replacing the human stromal component with mouse-derived stroma, direct *in vivo* passage allowed distinction of carcinoma cells having undergone EMT from stromal cells using a human specific anti-vimentin antibody. While high risk tumors manifested less infiltrative invasion in PDX form relative to the clinical specimen, dual-label IHC demonstrated their high content of vimentin-positive cells, which were rare or absent in low risk tumors (fig. 1A, supplementary fig. S1). Digital image analysis confirmed a wide, consistent disparity in vimentin staining between low and high risk groups (fig. 1B). Localization of the EMT transcription factor Zeb1 (33) to vimentin-positive tumor regions was observed in high risk PDXs (fig. 1C), where 72±7% and 55±5% of Zeb1-positive nuclei in respective OCTT2 and LNT14 PDXs contained vimentin-positive cytoplasm. This result supports a role for ongoing EMT in generating the vimentin-positive tumor cells within PDXs and is consistent with the mesenchymal-like gene expression profile shown previously for vimentin-positive subpopulations within cell lines (11). Overall, our findings provide evidence in human SCCs for an association between the abundance of mesenchymal-like cells and an infiltrative invasion pattern that might predispose to treatment failure.

Migration of mesenchymal-like cells in collagen-embedded spheroids generates infiltrative invasion

Cell lines OCTT2 and LNT14 were established successfully from the two SCCs with infiltrative invasion shown in fig. 1. To ensure clonal origin of heterogeneity arising from EMT within both lines, they were regrown from single colonies of FACS-purified E-cadherin-positive cells plated at clonal dilution. As demonstrated previously, E-cadherin-positive OCTT2 cells undergo EMT to produce a mesenchymal-like subset that allows this cell line to mimic the heterogeneity of its tumor of origin (11). Similar heterogeneity was noted in LNT14 cells (fig. 2A); yet E-cadherin positive LNT14 cells in culture underwent more rapid EMT, resulting in their dilution to 1-5% of cells in initial passages (data not shown). To maintain a smaller proportion of mesenchymal-like cells resembling that in the tumor of origin, LNT14 cells were FACS-purified for surface E-cadherin expression prior to use in subsequent *in vitro* studies.

Both cell lines formed spheroids that were invasive upon embedding in collagen matrix. In this system, OCTT2 cells produced two distinct invasion patterns: pushing fronts containing collectively migratory cells of epithelial morphology and infiltrative fronts arising from mesenchymal migration of spindle shaped cells (fig. 2B, top). DIC microscopy did not

clearly distinguish two distinct invasive fronts in LNT14 spheroids (fig. 2B, bottom). However, confocal IF subsequently identified E-cadherin positive cells collectively migrating as projections that maintain cell-cell contacts in both cell lines; this morphology contrasted with the appearance of the fusiform, vimentin-positive population entering the collagen as single cells (fig. 2C). These results showed that disparate invasion patterns are mediated in the spheroid model by epithelial and mesenchymal-like cellular components utilizing distinct modes of migration.

EGFR expression is decreased in the mesenchymal-like component of spheroids and PDXs

Prior results in conventional cell culture have shown decreased EGFR expression in the mesenchymal-like subpopulation by flow cytometry and western blot, which corresponds to diminished sensitivity to cetuximab (11). To assess EGFR expression by mesenchymal-like tumor cells in a more physiologic context, dual IF staining with vimentin was performed in OCTT2 and LNT14 cells grown as spheroids, as well as their PDXs of origin (fig. 3). In OCTT2 spheroids and PDXs, EGFR staining and vimentin staining were almost fully segregated from each other into distinct tumor cell subsets. LNT14 spheroids and PDXs also exhibited prominent EGFR down-regulation by such cells at the invasive periphery, while retaining EGFR expression in some vimentin-positive cells. Together, these results suggest that decreased EGFR expression in mesenchymal-like compartment may limit the efficacy of anti-EGFR drugs at the invasive front and thus mediate a shift in pattern of invasion upon treatment.

Targeting EGFR promotes an infiltrative stromal interface in spheroids containing mesenchymal-like cells

As shown previously for cetuximab (11), purified mesenchymal-like OCTT2 cells were resistant to erlotinib-induced growth inhibition relative to the E-cadherin-positive subset (supplementary fig. S2A). This resistance was consistent with their enrichment upon erlotinib treatment of unfractionated OCTT2 cells (supplementary fig. S2B). Based on these findings, the spheroid model was used to test whether currently used anti-EGFR drugs can alter SCC invasion pattern by creating a predominance of mesenchymal-like cells at the stromal interface. For this purpose, spheroids were treated with erlotinib, an EGFR-selective small molecule tyrosine kinase inhibitor, or cetuximab, a humanized anti-EGFR monoclonal antibody. Erlotinib produced growth inhibitory responses at an IC50 near 1 μM in LNT14 and OCTT2 cells, as well as in SCC13 cells (Fig. 4A), a cell line previously shown to lack detectable mesenchymal-like cells (11). Live-dead analysis of OCTT2 spheroids treated at this dose revealed individual fusiform cells infiltrating the stroma at the periphery despite central cell death (Fig. 4B), a finding suggesting a link between aggressive SCC invasion and resistance of mesenchymal-like cells to erlotinib. To validate this association, changes in distribution of E-cadherin positive versus mesenchymal-like cells were determined during spheroid invasion upon anti-EGFR therapy. Pre-existing subpopulations of E-cadherin and vimentin-positive cells were detectable in OCTT2 spheroids on day 0 after embedding, prior to invasion (Fig. 4C, top left). Over 3 days, untreated OCTT2 spheroids developed mixed invasive patterns comprised of pushing fronts mediated by the E-cadherin positive component, co-existent with infiltrative areas containing mesenchymal-like cells. Treatment of OCTT2 spheroids with erlotinib or cetuximab selectively diminished invasion of the E-cadherin positive cells, creating a stromal interface purely comprised of individual infiltrating mesenchymal-like cells, whose migration continued in presence of drug (Fig. 4C, right). Quantitative analysis of OCTT2 spheroid images confirmed a loss of E-cadherin staining area upon erlotinib or cetuximab-treatment, resulting in a proportional increase in representation of mesenchymal-like cells (Fig. 4C, bottom left). Erlotinib had similar effects in LNT14 spheroids, blocking migration by the E-cadherin-positive component to produce

an invasive front comprised solely of mesenchymal-like cells (Fig. 4D). In contrast, erlotinib treatment of SCC13 spheroids, which lack a mesenchymal-like subpopulation and invade in an exclusively pushing pattern, produced a dose-dependent inhibition of invasion, which was fully abrogated at 1μM (Fig. 4E). These findings further implicate mesenchymal-like cells as key mediators of infiltrative SCC invasion and indicate that their resistance to anti-EGFR drugs can promote formation of a high risk pattern of invasion in tumors where they pre-exist therapy.

In vivo cetuximab therapy in presence of mesenchymal-like cells potentiates their infiltrative invasion

Based upon these findings in spheroids, the effects of EGFR targeting upon invasion was evaluated further *in vivo* in presence or absence of a mesenchymal-like subpopulation, using xenografts of OCTT2 or SCC13 cells, respectively. Cetuximab treatment of established xenografts in NSG mice produced significant growth inhibition in both OCTT2 and SCC13 tumors (fig. 5A). While untreated OCTT2 xenografts maintained well-demarcated, pushing margins during growth, cetuximab therapy produced areas of invasion comprised of infiltration by narrow strands and small islands of tumor cells extending beyond the grossly visible tumor mass. Dual label IHC using human-specific anti-vimentin antibody showed vimentin expression in the isolated cells and small clusters predominating in these infiltrative regions of the invasive front (fig. 5B). Quantitative image analysis of OCTT2 xenografts confirmed an increase in vimentin staining upon cetuximab therapy that was significant at the invasive front but not in central areas of tumor (fig. 5C). By contrast, SCC13 xenografts showed growth inhibition in response to cetuximab without a shift in invasion pattern or emergence of a vimentin positive subpopulation (fig. 5D). Together, these results offer *in vivo* evidence of EGFR inhibition producing more aggressive SCC invasion when mesenchymal-like tumor cells are present. They further support the fidelity of collagen-embedded spheroids for modeling the changes in tumor cell subpopulation dynamics that impact invasion during targeted therapy.

Discussion

SCCs have diverse biologic traits, ranging from well-circumscribed lesions curable by excision alone to aggressive tumors showing infiltrative invasion, prominent stromal reactions, and early metastasis. Whether EMT drives aggressive carcinoma behavior remains an area of controversy (34), in part because discrimination of tumor cells undergoing EMT in tissues is impaired by their markers being shared by human stromal cells. To address this limitation here, human stromal elements in primary head and neck SCCs were replaced with mouse-derived components by *in vivo* passage as PDXs. Although the mouse stromal environment allowed less SCC infiltration, these PDXs provided new evidence that tumor cells having undergone EMT are highly represented within the infiltrative subset of tumors. We demonstrated that relative resistance of these mesenchymal-like cells to EGFR inhibition can lead to current EGFR-targeted drugs simultaneously causing partial tumor regression and promoting infiltrative histology. These results provide a novel link between therapeutic EGFR inhibition and promotion of a histology at the SCC invasive front that, in untreated SCCs, has been associated with aggressive clinical behavior. Importantly, enhanced tumor progression and poorer clinical outcomes in patients treated with EGFR inhibitors have not been shown and cannot be concluded here.

Our results support a model in which a large pre-existing subpopulation of mesenchymal-like tumor cells is necessary for cetuximab or erlotinib to produce more infiltrative invasion during tumor regression (fig. 6). In cell lines containing large mesenchymal-like subsets, the effect appears mediated primarily by sensitivity of the epithelial subpopulation to growth

inhibition during EGFR targeting. A paucity of erlotinib-induced apoptosis in conventional culture (data not shown) was contrary to the cell death observed in the spheroid format, which commonly alters drug responses and may more closely model *in vivo* biology (35, 36). An alternate possibility is that EGFR inhibition does not merely enrich resistant mesenchymal-like cells but also promotes expansion of this cell pool by driving ongoing EMT, thus allowing further escape from EGFR dependence. Studies indicating a requirement for ongoing growth factor signaling for EMT (37-39) however predict that EGFR targeting would instead block further EMT-mediated expansion of the mesenchymal-like subset, as illustrated in our working model. Attempts to test this hypothesis directly by generating spheroids from purified E-cadherin-positive OCTT2 cells were inconclusive, as these purified cells rapidly repopulated the mesenchymal-like compartment even in the presence of erlotinib (data not shown). This outcome may reflect a subset of E-cadherin-positive cells already being committed to EMT at the time of FACS purification.

Our results lead to speculation that anti-EGFR therapy disparately impacts local progression of two distinct SCC sub-types defined by the presence or absence of mesenchymal-like tumor cells. However their relevance to the ongoing discussion regarding the role of EMT in metastatic progression is unclear (34). Notably, the patients of origin for 5 of the 6 PDXs in which mesenchymal-like cells were rare or absent still had nodal metastases at diagnosis in this study (Table S1). These findings may indicate that the key components of the EMT program required for metastatic dissemination are not discretely encompassed by the subpopulation phenotype as defined here. Indeed, no single marker is likely to fully capture a range of phenotypes generated by the EMT program, as evidenced here by incomplete overlap between vimentin and Zeb-1 markers.

Detecting mesenchymal-like differentiation may ultimately prove valuable in rational drug selection for a malignancy presently lacking in biomarkers to guide use of anti-EGFR therapy. Despite ample evidence associating EGFR gene amplification and/or overexpression with poor prognosis in head and neck SCCs (40, 41), gene copy number and IHC detection have failed to predict the response to EGFR inhibition for individual patients (42, 43). A few genetic alterations are proven to predict sensitivity or resistance to anti-EGFR therapy, specifically EGFR or K-Ras activating mutations in lung or colon carcinomas, respectively (44-46); however, these mutations are seldom found in SCCs, with exception of the squamous subgroup of non-small cell lung cancers. The paradigm of directing SCC therapy at overall tumor cell phenotypes rather than individual driving oncogenes is advanced by the recently published cancer genome for head and neck SCC, which largely fails to identify new, readily targetable molecules among common mutations (47). Based on the dependence of EMT on MAP kinase signals (38, 39), we speculate that mesenchymal-like cells are more likely to arise within poorer prognosis tumors with highly activated EGFR signaling. Therefore development of mesenchymal-like cells with aggressive, drug-resistant features indeed may directly contribute to poorer prognosis in tumors expressing high overall EGFR levels, despite EGFR down-regulation by the mesenchymal-like subset itself.

The finding of infiltrative invasion in association with abundant mesenchymal-like cells may have additional implications for surgical therapy. Highly infiltrative tumors with poorly defined boundaries may recur even after wide margin resections, while close margins can achieve tumor control even for certain locally advanced head and neck SCCs (48). Although avoiding the morbidity of a wide resection would be desirable for the less infiltrative tumors, the inability of diagnostic biopsy specimens to represent the invasive front adequately prevents use of this feature in clinical decision making. Figures 1 and S1 suggest that mesenchymal-like differentiation within SCCs manifests as infiltrative behavior at the invasive front but is not limited to the tumor-stromal interface. The potential for detection of

mesenchymal-like differentiation within biopsies to serve as a reliable indicator of infiltrative histology therefore warrants further assessment of our findings here in larger patient populations. Finally, the increased infiltration by mesenchymal-like cells detected here in an SCC treated with cetuximab has bearing on the longstanding question of how neoadjuvant chemotherapy alters subsequent surgical resection margins. This issue is particularly pertinent to therapy of early stage esophageal SCC, where induction chemotherapy prior to esophagectomy improves survival (49) and has become widely practiced. Testing the hypothesis that surgical margins for tumors containing abundant mesenchymal-like cells are not improved by neoadjuvant use of EGFR inhibitors or other drugs could ultimately spare induction chemotherapy for certain patient subgroups.

Supplementary Material

Refer to Web version on PubMed Central for supplementary material.

Acknowledgments

This work is supported by NIH grants K08 DE022842 (D Basu), P01 CA098101 (P Gimotty, AK Rustgi, JA Diehl, H Nakagawa, M Herlyn) including its Molecular Pathology, Molecular Biology, and Biostatistical Cores, and P30 DK050306 and its Cell Culture Core. A Bewley and S Sperry were supported by awards from the AAO-HNS.

Grant Support: This work is supported by NIH grants K08 DE022842 (D Basu), P01 CA098101 (P Gimotty, AK Rustgi, JA Diehl, H Nakagawa, M Herlyn), and P30 DK050306, as well as AAO-HNS Resident Research Awards (A Bewley, S Sperry).

References

1. Brandwein-Gensler M, Teixeira MS, Lewis CM, Lee B, Rolnitzky L, Hille JJ, et al. Oral squamous cell carcinoma: histologic risk assessment, but not margin status, is strongly predictive of local disease-free and overall survival. Am J Surg Pathol. 2005; 29:167–78. [PubMed: 15644773]
2. Spiro RH, Guillamondegui O Jr. Paulino AF, Huvos AG. Pattern of invasion and margin assessment in patients with oral tongue cancer. Head Neck. 1999; 21:408–13. [PubMed: 10402520]
3. Brandwein-Gensler M, Smith RV, Wang B, Penner C, Theilken A, Broughel D, et al. Validation of the histologic risk model in a new cohort of patients with head and neck squamous cell carcinoma. Am J Surg Pathol. 2010; 34:676–88. [PubMed: 20414102]
4. Li Y, Bai S, Carroll W, Dayan D, Dort JC, Heller K, et al. Validation of the Risk Model: High-Risk Classification and Tumor Pattern of Invasion Predict Outcome for Patients with Low-Stage Oral Cavity Squamous Cell Carcinoma. Head Neck Pathol. Dec.2012 Epub.
5. Ooki A, Yamashita K, Kobayashi N, Katada N, Sakuramoto S, Kikuchi S, et al. Lymph node metastasis density and growth pattern as independent prognostic factors in advanced esophageal squamous cell carcinoma. World J Surg. 2007; 31:2184–91. [PubMed: 17721721]
6. Ito E, Ozawa S, Kijima H, Kazuno A, Nishi T, Chino O, et al. New invasive patterns as a prognostic factor for superficial esophageal cancer. J Gastroenterol. 2012; 47:1279–89. [PubMed: 22576024]
7. Horn LC, Fischer U, Raptis G, Bilek K, Hentschel B, Richter CE, et al. Pattern of invasion is of prognostic value in surgically treated cervical cancer patients. Gynecol Oncol. 2006; 103:906–11. [PubMed: 16876852]
8. Guimaraes GC, Lopes A, Campos RS, Zequi Sde C, Leal ML, Carvalho AL, et al. Front pattern of invasion in squamous cell carcinoma of the penis: new prognostic factor for predicting risk of lymph node metastases. Urology. 2006; 68:148–53. [PubMed: 16844455]
9. Sarbia M, Bittinger F, Porschen R, Dutkowski P, Willers R, Gabbert HE. Prognostic value of histopathologic parameters of esophageal squamous cell carcinoma. Cancer. 1995; 76:922–7. [PubMed: 8625216]
10. Po Wing Yuen A, Lam KY, Lam LK, Ho CM, Wong A, Chow TL, et al. Prognostic factors of clinically stage I and II oral tongue carcinoma-A comparative study of stage, thickness, shape,

growth pattern, invasive front malignancy grading, Martinez-Gimeno score, and pathologic features. Head Neck. 2002; 24:513–20. [PubMed: 12112547]

11. Basu D, Nguyen TT, Montone KT, Zhang G, Wang LP, Diehl JA, et al. Evidence for mesenchymal-like sub-populations within squamous cell carcinomas possessing chemoresistance and phenotypic plasticity. Oncogene. 2010; 29:4170–82. [PubMed: 20498638]
12. Basu D, Montone KT, Wang LP, Gimotty PA, Hammond R, Diehl JA, et al. Detecting and targeting mesenchymal-like subpopulations within squamous cell carcinomas. Cell Cycle. 2011; 10:2008–16. [PubMed: 21558812]
13. Guarino M, Rubino B, Ballabio G. The role of epithelial-mesenchymal transition in cancer pathology. Pathology. 2007; 39:305–18. [PubMed: 17558857]
14. Kupferman ME, Jiffar T, El-Naggar A, Yilmaz T, Zhou G, Xie T, et al. TrkB induces EMT and has a key role in invasion of head and neck squamous cell carcinoma. Oncogene. 2010; 29:2047–59. [PubMed: 20101235]
15. Marsh D, Suchak K, Moutasim KA, Vallath S, Hopper C, Jerjes W, et al. Stromal features are predictive of disease mortality in oral cancer patients. J Pathol. 2011; 223:470–81. [PubMed: 21294121]
16. Yang J, Weinberg RA. Epithelial-mesenchymal transition: at the crossroads of development and tumor metastasis. Dev Cell. 2008; 14:818–29. [PubMed: 18539112]
17. Mani SA, Guo W, Liao MJ, Eaton EN, Ayyanan A, Zhou AY, et al. The epithelial-mesenchymal transition generates cells with properties of stem cells. Cell. 2008; 133:704–15. [PubMed: 18485877]
18. Wolf K, Wu YI, Liu Y, Geiger J, Tam E, Overall C, et al. Multi-step pericellular proteolysis controls the transition from individual to collective cancer cell invasion. Nat Cell Biol. 2007; 9:893–904. [PubMed: 17618273]
19. Sanz-Moreno V, Marshall CJ. The plasticity of cytoskeletal dynamics underlying neoplastic cell migration. Curr Opin Cell Biol. 2010; 22:690–6. [PubMed: 20829016]
20. Yang WH, Lan HY, Huang CH, Tai SK, Tzeng CH, Kao SY, et al. RAC1 activation mediates Twist1-induced cancer cell migration. Nat Cell Biol. 2012; 14:366–74. [PubMed: 22407364]
21. Wyckoff JB, Pinner SE, Gschmeissner S, Condeelis JS, Sahai E. ROCK- and myosin-dependent matrix deformation enables protease-independent tumor-cell invasion in vivo. Curr Biol. 2006; 16:1515–23. [PubMed: 16890527]
22. Paez-Ribes M, Allen E, Hudock J, Takeda T, Okuyama H, Vinals F, et al. Antiangiogenic therapy elicits malignant progression of tumors to increased local invasion and distant metastasis. Cancer Cell. 2009; 15:220–31. [PubMed: 19249680]
23. Karamouzis MV, Grandis JR, Argiris A. Therapies directed against epidermal growth factor receptor in aerodigestive carcinomas. JAMA. 2007; 298:70–82. [PubMed: 17609492]
24. Barr S, Thomson S, Buck E, Russo S, Petti F, Sujka-Kwok I, et al. Bypassing cellular EGF receptor dependence through epithelial-to-mesenchymal-like transitions. Clin Exp Metastasis. 2008; 25:685–93. [PubMed: 18236164]
25. Thomson S, Buck E, Petti F, Griffin G, Brown E, Ramnarine N, et al. Epithelial to mesenchymal transition is a determinant of sensitivity of non-small-cell lung carcinoma cell lines and xenografts to epidermal growth factor receptor inhibition. Cancer Res. 2005; 65:9455–62. [PubMed: 16230409]
26. Haddad Y, Choi W, McConkey DJ. Delta-crystallin enhancer binding factor 1 controls the epithelial to mesenchymal transition phenotype and resistance to the epidermal growth factor receptor inhibitor erlotinib in human head and neck squamous cell carcinoma lines. Clin Cancer Res. 2009; 15:532–42. [PubMed: 19147758]
27. Yauch RL, Januario T, Eberhard DA, Cavet G, Zhu W, Fu L, et al. Epithelial versus mesenchymal phenotype determines in vitro sensitivity and predicts clinical activity of erlotinib in lung cancer patients. Clin Cancer Res. 2005; 11:8686–98. [PubMed: 16361555]
28. Frederick BA, Helfrich BA, Coldren CD, Zheng D, Chan D, Bunn PA Jr. et al. Epithelial to mesenchymal transition predicts gefitinib resistance in cell lines of head and neck squamous cell carcinoma and non-small cell lung carcinoma. Mol Cancer Ther. 2007; 6:1683–91. [PubMed: 17541031]

29. La Fleur L, Johansson AC, Roberg K. A CD44high/EGFRlow subpopulation within head and neck cancer cell lines shows an epithelial-mesenchymal transition phenotype and resistance to treatment. PLoS One. 2012; 7:e44071. [PubMed: 23049743]
30. Smalley KS, Haass NK, Brafford PA, Lioni M, Flaherty KT, Herlyn M. Multiple signaling pathways must be targeted to overcome drug resistance in cell lines derived from melanoma metastases. Mol Cancer Ther. 2006; 5:1136–44. [PubMed: 16731745]
31. Andl CD, Mizushima T, Nakagawa H, Oyama K, Harada H, Chruma K, et al. Epidermal growth factor receptor mediates increased cell proliferation, migration, and aggregation in esophageal keratinocytes in vitro and in vivo. J Biol Chem. 2003; 278:1824–30. [PubMed: 12435727]
32. Darling DS, Stearman RP, Qi Y, Qiu MS, Feller JP. Expression of Zfhep/deltaEF1 protein in palate, neural progenitors, and differentiated neurons. Gene Expr Patterns. 2003; 3:709–17. [PubMed: 14643678]
33. Ohashi S, Natsuizaka M, Naganuma S, Kagawa S, Kimura S, Itoh H, et al. A NOTCH3-mediated squamous cell differentiation program limits expansion of EMT-competent cells that express the ZEB transcription factors. Cancer Res. 2011; 71:6836–47. [PubMed: 21890822]
34. Ledford H. Cancer theory faces doubts. Nature. 2011; 472:273. [PubMed: 21512545]
35. Friedrich J, Seidel C, Ebner R, Kunz-Schughart LA. Spheroid-based drug screen: considerations and practical approach. Nat Protoc. 2009; 4:309–24. [PubMed: 19214182]
36. LaBarbera DV, Reid BG, Yoo BH. The multicellular tumor spheroid model for high-throughput cancer drug discovery. Expert Opin Drug Discov. 2012; 7:819–30. [PubMed: 22788761]
37. Zhang D, LaFortune TA, Krishnamurthy S, Esteva FJ, Cristofanilli M, Liu P, et al. Epidermal growth factor receptor tyrosine kinase inhibitor reverses mesenchymal to epithelial phenotype and inhibits metastasis in inflammatory breast cancer. Clin Cancer Res. 2009; 15:6639–48. [PubMed: 19825949]
38. Shin S, Dimitri CA, Yoon SO, Dowdle W, Blenis J. ERK2 but not ERK1 induces epithelial-to-mesenchymal transformation via DEF motif-dependent signaling events. Mol Cell. 2010; 38:114–27. [PubMed: 20385094]
39. Xie L, Law BK, Chytil AM, Brown KA, Aakre ME, Moses HL. Activation of the Erk pathway is required for TGF-beta1-induced EMT in vitro. Neoplasia. 2004; 6:603–10. [PubMed: 15548370]
40. Chung CH, Ely K, McGavran L, Varella-Garcia M, Parker J, Parker N, et al. Increased epidermal growth factor receptor gene copy number is associated with poor prognosis in head and neck squamous cell carcinomas. J Clin Oncol. 2006; 24:4170–6. [PubMed: 16943533]
41. Wheeler S, Siwak DR, Chai R, LaValle C, Seethala RR, Wang L, et al. Tumor epidermal growth factor receptor and EGFR PY1068 are independent prognostic indicators for head and neck squamous cell carcinoma. Clin Cancer Res. 2012; 18:2278–89. [PubMed: 22351687]
42. Fischer C, Zlobec I, Stockli E, Probst S, Storck C, Tornillo L, et al. Is immunohistochemical epidermal growth factor receptor expression overestimated as a prognostic factor in head-neck squamous cell carcinoma? A retrospective analysis based on a tissue microarray of 365 carcinomas. Hum Pathol. 2008; 39:1527–34. [PubMed: 18620726]
43. Licitra L, Mesia R, Rivera F, Remenar E, Hitt R, Erfan J, et al. Evaluation of EGFR gene copy number as a predictive biomarker for the efficacy of cetuximab in combination with chemotherapy in the first-line treatment of recurrent and/or metastatic squamous cell carcinoma of the head and neck: EXTREME study. Ann Oncol. 2011; 22:1078–87. [PubMed: 21048039]
44. Sequist LV, Martins RG, Spigel D, Grunberg SM, Spira A, Janne PA, et al. First-line gefitinib in patients with advanced non-small-cell lung cancer harboring somatic EGFR mutations. J Clin Oncol. 2008; 26:2442–9. [PubMed: 18458038]
45. Karapetis CS, Khambata-Ford S, Jonker DJ, O'Callaghan CJ, Tu D, Tebbutt NC, et al. K-ras mutations and benefit from cetuximab in advanced colorectal cancer. N Engl J Med. 2008; 359:1757–65. [PubMed: 18946061]
46. Licitra L, Storkel S, Kerr KM, Van Cutsem E, Pirker R, Hirsch FR, et al. Predictive value of epidermal growth factor receptor expression for first-line chemotherapy plus cetuximab in patients with head and neck and colorectal cancer: analysis of data from the EXTREME and CRYSTAL studies. Eur J Cancer. 2013; 49:1161–8. [PubMed: 23265711]

47. Stransky N, Egloff AM, Tward AD, Kostic AD, Cibulskis K, Sivachenko A, et al. The mutational landscape of head and neck squamous cell carcinoma. Science. 2011; 333:1157–60. [PubMed: 21798893]

48. Hinni ML, Ferlito A, Brandwein-Gensler MS, Takes RP, Silver CE, Westra WH, et al. Surgical margins in head and neck cancer: A contemporary review. Head Neck. Sept.2012 Epub.

49. Okines A, Sharma B, Cunningham D. Perioperative management of esophageal cancer. Nat Rev Clin Oncol. 2010; 7:231–8. [PubMed: 20212503]

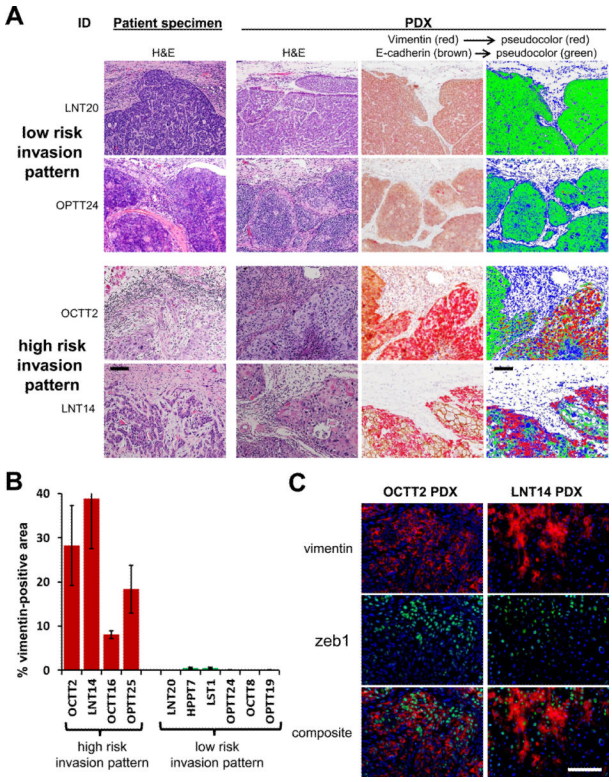

Figure 1. Abundant mesenchymal-like cells are present in PDXs of SCCs with infiltrative invasion

A, Micrographs are of representative primary SCCs grouped by invasion pattern and their corresponding PDXs. Dual label IHC of PDXs for E-cadherin (brown) and vimentin (red) is shown together with digitally pseudo-colored images, in which E-cadherin is green, vimentin is red, and hematoxylin is blue. 20x. **B,** Vimentin positive area is compared between groups with high and low risk invasion patterns, quantitated as a percentage of total (E-cadherin+vimentin) staining area. Areas are defined as the mean ± SEM of three 40x fields. $P<1\times10^{-6}$ between groups. **C,** IF costaining of vimentin (red) and zeb-1 (green) is shown in sections of PDXs with high risk invasion patterns. 40x. Bars=100μm.

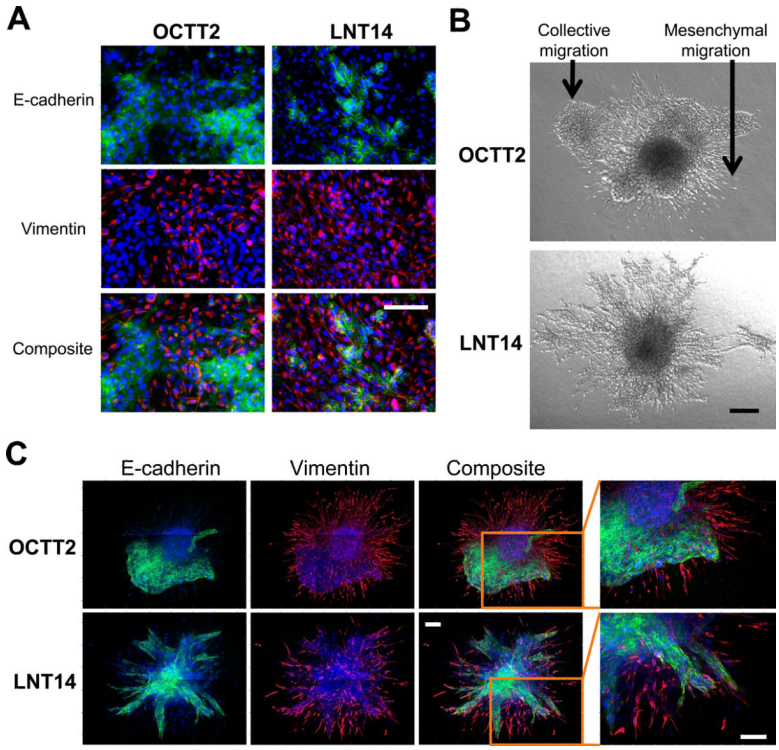

Figure 2. Infiltrative invasion of SCC spheroids arises from migration of mesenchymal-like cells

A, IF micrographs are of OCTT2 and LNT14 cell lines stained for 4',6-diamidino-2-phenylindole (DAPI, blue), E-cadherin (green), and vimentin (red). 20x. **B,** 4x DIC micrographs of OCTT2 and LNT14 spheroids. **C,** Confocal IF of OCTT2 and LNT14 spheroids stained as in A. Images are mosaics of multiple 10x fields. Bars=200μm.

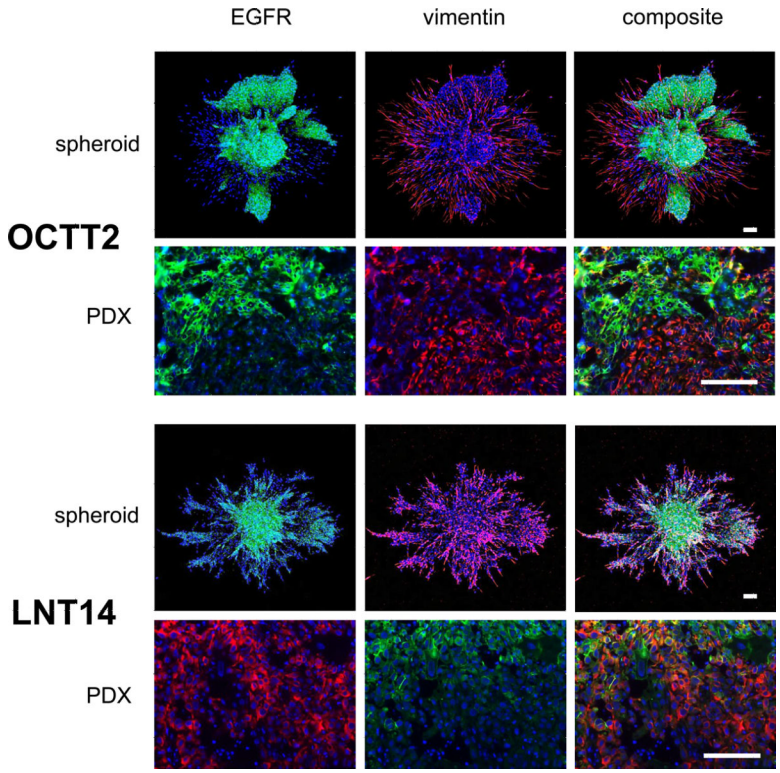

Figure 3. EGFR expression is reduced in mesenchymal-like cells within SCC spheroids and PDXs

OCTT2 and LNT14 spheroids (top panels, 10x) and PDX tissue sections (bottom panels, 40x) are stained for DAPI (blue), EGFR (green), and vimentin (red). Confocal IF images of spheroids are 10x. Images are representative of ≥3 independently stained samples. Bars=100μm.

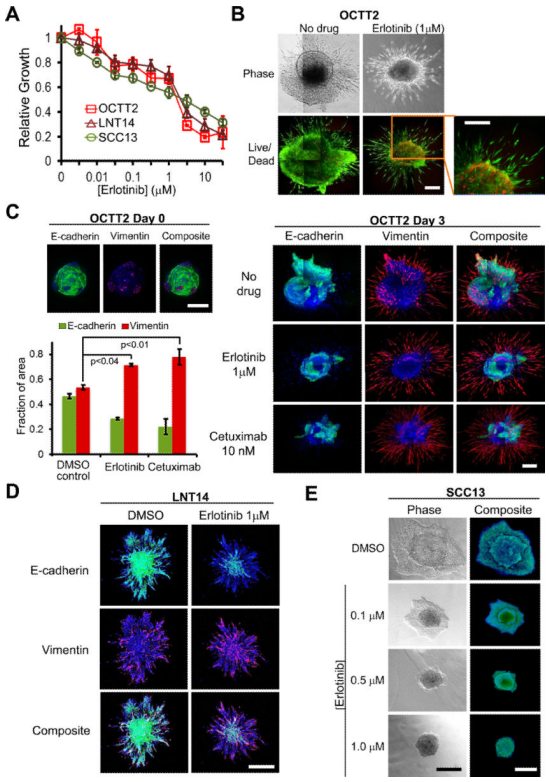

Figure 4. EGFR inhibition promotes an infiltrative invasion pattern in spheroids containing mesenchymal-like cells

A, Drug-induced growth inhibition of OCTT2, LNT14, and SCC13 cells was measured by MTS assay following 72 hrs. erlotinib treatment. **B,** OCTT2 spheroids were grown 72 hrs in presence and absence of erlotinib. Images are mosaics of multiple 10x light (top) and IF (bottom) confocal fields. Bottom panels show calcein AM (green) and ethidium homodimer (red) live/dead staining. **C,** Confocal IF images of OCTT2 spheroids stained for E-cadherin (green), vimentin (red), and DAPI (blue) are shown at time point 0 (left top, 10x) and after 72 hrs. of erlotinib or cetuximab treatment (right, 10x mosaic images). Graph illustrates shift in vimentin or E-cadherin staining with spheroid treatment, measured as a percentage of total (E-cadherin+vimentin) staining area and represented as mean ± SEM from 3 separate spheroids. **D,** 10x confocal IF images are shown of LNT14 spheroids erlotinib-treated and stained as in C. **E,** 4x DIC (left) and 10x confocal IF (right) images of SCC13 spheroids are shown after 72 hrs. exposure to indicated erlotinib doses and dual IF staining as in C. Bars=400μm. Results are representative of ≥3 independent experiments.

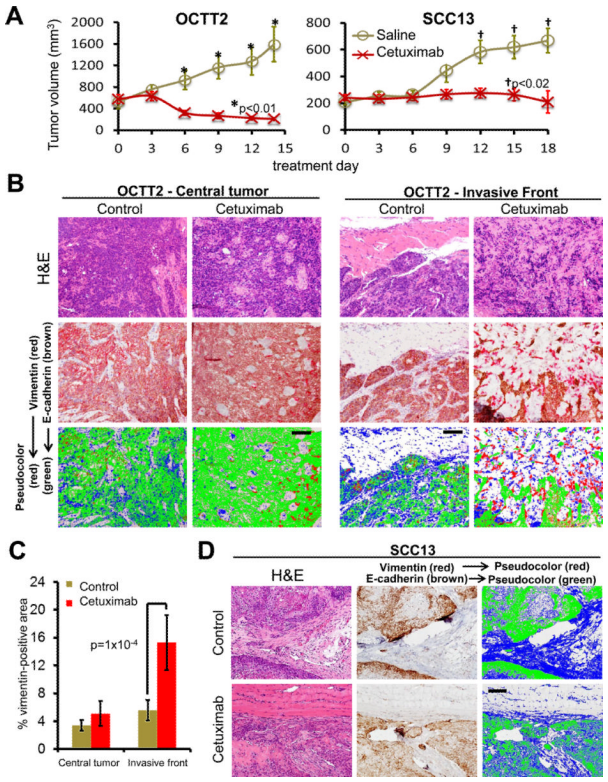

Figure 5. An infiltrative front comprised of mesenchymal-like cells is potentiated by *in vivo* cetuximab therapy

A, Subcutaneous xenografts of 1×10^6 OCTT2 or SCC13 cells were grown for 14 (OCTT2) or 28 (SCC13) days, and mice with established tumors were subsequently treated with cetuximab or saline every 3 days over 5 (OCTT2) or 6 (SCC13) doses (n=5/group). Tumor volume is plotted during treatment. **B,** Dual label IHC of treated and control OCTT2 tumors for E-cadherin (brown) and vimentin (red) is shown at the central tumor (left) and invasive front (right). Pseudo-color images show E-cadherin in green, vimentin in red, and hematoxylin in blue. **C,** Vimentin staining area was compared between treated and control tumors in central and peripheral zones, quantitated as a percentage of total (E-cadherin +vimentin) staining area. Values respresent mean ± SEM of 25 40x fields (5 fields per tumor). **D,** Dual label IHC and pseudocolor images of treated and control SCC13 tumors are shown at the invasive front, as in C. Images are 20x. Bars=100μm.

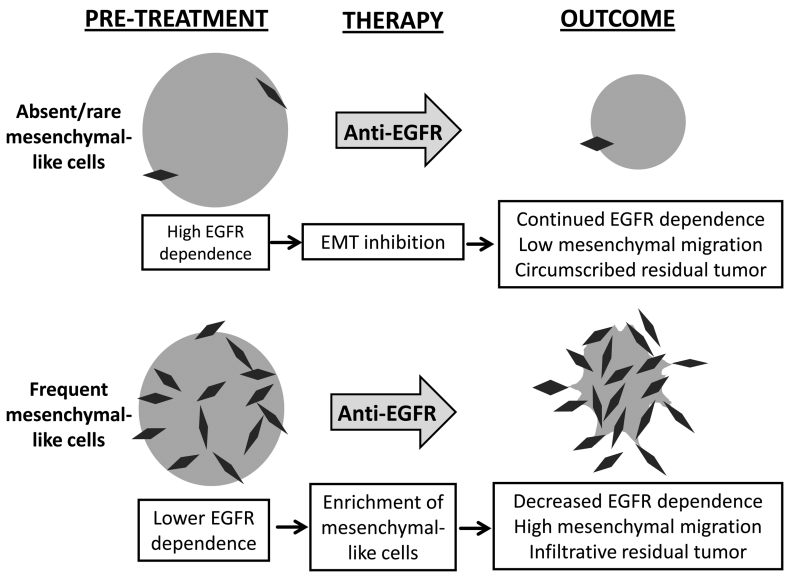

Figure 6.
Model for EGFR inhibitor responses in SCCs containing abundant versus rare mesenchymal-like cells